Physics Letters B 770 (2017) 418–425

Contents lists available at ScienceDirect

Physics Letters B

www.elsevier.com/locate/physletb

Measurement of the $\omega \to \pi^+\pi^-\pi^0$ Dalitz plot distribution

The WASA-at-COSY Collaboration

P. Adlarson [a,1], W. Augustyniak [b], W. Bardan [c], M. Bashkanov [d], F.S. Bergmann [e], M. Berłowski [f], H. Bhatt [g], A. Bondar [h,i], M. Büscher [j,2,3], H. Calén [a], I. Ciepał [k], H. Clement [l,m], E. Czerwiński [c], K. Demmich [e], R. Engels [j], A. Erven [n], W. Erven [n], W. Eyrich [o], P. Fedorets [j,p], K. Föhl [q], K. Fransson [a], F. Goldenbaum [j], A. Goswami [j,r], K. Grigoryev [j,s,4], C.-O. Gullström [a], L. Heijkenskjöld [a,*], V. Hejny [j], N. Hüsken [e], L. Jarczyk [c], T. Johansson [a], B. Kamys [c], G. Kemmerling [n,5], F.A. Khan [j], G. Khatri [c,6], A. Khoukaz [e], O. Khreptak [c], D.A. Kirillov [t], S. Kistryn [c], H. Kleines [n,5], B. Kłos [u], W. Krzemień [f], P. Kulessa [k], A. Kupść [a,f], A. Kuzmin [h,i], K. Lalwani [v], D. Lersch [j], B. Lorentz [j], A. Magiera [c], R. Maier [j,w], P. Marciniewski [a], B. Mariański [b], H.-P. Morsch [b], P. Moskal [c], H. Ohm [j], E. Perez del Rio [l,m,7], N.M. Piskunov [t], D. Prasuhn [j], D. Pszczel [a,f], K. Pysz [k], A. Pyszniak [a,c], J. Ritman [j,w,x], A. Roy [r], Z. Rudy [c], O. Rundel [c], S. Sawant [g,j,**], S. Schadmand [j], I. Schätti-Ozerianska [c], T. Sefzick [j], V. Serdyuk [j], B. Shwartz [h,i], K. Sitterberg [e], T. Skorodko [l,m,y], M. Skurzok [c], J. Smyrski [c], V. Sopov [p], R. Stassen [j], J. Stepaniak [f], E. Stephan [u], G. Sterzenbach [j], H. Stockhorst [j], H. Ströher [j,w], A. Szczurek [k], A. Trzciński [b], R. Varma [g], M. Wolke [a], A. Wrońska [c], P. Wüstner [n], A. Yamamoto [z], J. Zabierowski [aa], M.J. Zieliński [c], J. Złomańczuk [a], P. Żuprański [b], M. Żurek [j]

[a] Division of Nuclear Physics, Department of Physics and Astronomy, Uppsala University, Box 516, 75120 Uppsala, Sweden
[b] Department of Nuclear Physics, National Centre for Nuclear Research, ul. Hoza 69, 00-681, Warsaw, Poland
[c] Institute of Physics, Jagiellonian University, prof. Stanisława Łojasiewicza 11, 30-348 Kraków, Poland
[d] School of Physics and Astronomy, University of Edinburgh, James Clerk Maxwell Building, Peter Guthrie Tait Road, Edinburgh EH9 3FD, United Kingdom
[e] Institut für Kernphysik, Westfälische Wilhelms-Universität Münster, Wilhelm-Klemm-Str. 9, 48149 Münster, Germany
[f] High Energy Physics Department, National Centre for Nuclear Research, ul. Hoza 69, 00-681, Warsaw, Poland
[g] Department of Physics, Indian Institute of Technology Bombay, Powai, Mumbai 400076, Maharashtra, India
[h] Budker Institute of Nuclear Physics of SB RAS, 11 akademika Lavrentieva prospect, Novosibirsk, 630090, Russia
[i] Novosibirsk State University, 2 Pirogova Str., Novosibirsk, 630090, Russia
[j] Institut für Kernphysik, Forschungszentrum Jülich, 52425 Jülich, Germany
[k] The Henryk Niewodniczański Institute of Nuclear Physics, Polish Academy of Sciences, 152 Radzikowskiego St, 31-342 Kraków, Poland
[l] Physikalisches Institut, Eberhard-Karls-Universität Tübingen, Auf der Morgenstelle 14, 72076 Tübingen, Germany
[m] Kepler Center for Astro and Particle Physics, Eberhard Karls University Tübingen, Auf der Morgenstelle 14, 72076 Tübingen, Germany
[n] Zentralinstitut für Engineering, Elektronik und Analytik, Forschungszentrum Jülich, 52425 Jülich, Germany
[o] Physikalisches Institut, Friedrich-Alexander-Universität Erlangen–Nürnberg, Erwin-Rommel-Str. 1, 91058 Erlangen, Germany
[p] Institute for Theoretical and Experimental Physics, State Scientific Center of the Russian Federation, Bolshaya Cheremushkinskaya 25, 117218 Moscow, Russia
[q] II. Physikalisches Institut, Justus-Liebig-Universität Gießen, Heinrich-Buff-Ring 16, 35392 Giessen, Germany
[r] Department of Physics, Indian Institute of Technology Indore, Khandwa Road, Indore 452017, Madhya Pradesh, India

* Corresponding author.
** Corresponding author at: Department of Physics, Indian Institute of Technology Bombay, Powai, Mumbai 400076, Maharashtra, India.
E-mail addresses: lena.heijkenskjold@physics.uu.se (L. Heijkenskjöld), siddhesh.sawant@iitb.ac.in (S. Sawant).
[1] Present address: Institut für Kernphysik, Johannes-Gutenberg-Universität Mainz, Johann-Joachim-Becher Weg 45, 55128 Mainz, Germany.
[2] Present address: Peter Grünberg Institut, PGI-6 Elektronische Eigenschaften, Forschungszentrum Jülich, 52425 Jülich, Germany.
[3] Present address: Institut für Laser- und Plasmaphysik, Heinrich-Heine Universität Düsseldorf, Universitätsstr. 1, 40225 Düsseldorf, Germany.
[4] Present address: III. Physikalisches Institut B, Physikzentrum, RWTH Aachen, 52056 Aachen, Germany.
[5] Present address: Jülich Centre for Neutron Science JCNS, Forschungszentrum Jülich, 52425 Jülich, Germany.
[6] Present address: Department of Physics, Harvard University, 17 Oxford St., Cambridge, MA 02138, USA.
[7] Present address: INFN, Laboratori Nazionali di Frascati, Via E. Fermi, 40, 00044 Frascati (Roma), Italy.

http://dx.doi.org/10.1016/j.physletb.2017.03.050

[s] High Energy Physics Division, Petersburg Nuclear Physics Institute, Orlova Rosha 2, Gatchina, Leningrad district 188300, Russia
[t] Veksler and Baldin Laboratory of High Energiy Physics, Joint Institute for Nuclear Physics, Joliot-Curie 6, 141980 Dubna, Moscow region, Russia
[u] August Chełkowski Institute of Physics, University of Silesia, Uniwersytecka 4, 40-007, Katowice, Poland
[v] Department of Physics, Malaviya National Institute of Technology Jaipur, 302017, Rajasthan, India
[w] JARA-FAME, Jülich Aachen Research Alliance, Forschungszentrum Jülich, 52425 Jülich, and RWTH Aachen, 52056 Aachen, Germany
[x] Institut für Experimentalphysik I, Ruhr-Universität Bochum, Universitätsstr. 150, 44780 Bochum, Germany
[y] Department of Physics, Tomsk State University, 36 Lenina Avenue, Tomsk, 634050, Russia
[z] High Energy Accelerator Research Organisation KEK, Tsukuba, Ibaraki 305-0801, Japan
[aa] Department of Astrophysics, National Centre for Nuclear Research, Box 447, 90-950 Łódź, Poland

B. Kubis [ab], S. Leupold [ac]

[ab] Helmholtz-Institut für Strahlen- und Kernphysik, Rheinische Friedrich-Wilhelms-Universität Bonn, Nußallee 14–16, 53115 Bonn, Germany
[ac] Division of Nuclear Physics, Department of Physics and Astronomy, Uppsala University, Box 516, 75120 Uppsala, Sweden

ARTICLE INFO

Article history:
Received 10 October 2016
Received in revised form 29 January 2017
Accepted 8 March 2017
Available online 25 April 2017
Editor: V. Metag

Keywords:
Decays of other mesons
Meson–meson interactions
Light mesons

ABSTRACT

Using the production reactions $pd \to {}^3\mathrm{He}\,\omega$ and $pp \to pp\omega$, the Dalitz plot distribution for the $\omega \to \pi^+\pi^-\pi^0$ decay is studied with the WASA detector at COSY, based on a combined data sample of $(4.408 \pm 0.042) \times 10^4$ events. The Dalitz plot density is parametrised by a product of the P-wave phase space and a polynomial expansion in the normalised polar Dalitz plot variables Z and ϕ. For the first time, a deviation from pure P-wave phase space is observed with a significance of 4.1σ. The deviation is parametrised by a linear term $1 + 2\alpha Z$, with α determined to be $+0.147 \pm 0.036$, consistent with the expectations of ρ-meson-type final-state interactions of the P-wave pion pairs.

1. Introduction

The present work and foreseeable follow-ups are based on two motivations: 1. To check and improve on our understanding of the importance of hadronic final-state interactions for the structure and decays of hadrons. 2. To improve the Standard Model prediction for the gyromagnetic ratio of the muon [1]. The present work accomplishes the first task concerning the Dalitz decay of the ω meson into three pions; it also constitutes a significant step forward towards providing improved hadronic input for the second task. In the following we shall discuss the two tasks in more detail.

The ω-meson resonance was discovered in 1961 [2]. Its main decay branch is $\omega \to \pi^+\pi^-\pi^0$, with a branching ratio of $\mathrm{BR} = (89.2 \pm 0.7)\%$. By now it is well established that the ω meson has spin-parity $J^P = 1^-$ [3]. As a consequence, the combination of Bose, isospin, and parity symmetry of the strong interaction demands that for the decay $\omega \to \pi^+\pi^-\pi^0$ every pion pair is in a state of odd relative orbital angular momentum. Given the limited phase space of the decay one can safely assume the P-wave to be the dominant partial wave.[8] If a pion pair is in a P-wave state, then the third pion will be in P-wave state relative to the pair. This "P-wave phase space" distribution has been confirmed experimentally. Historically the P-wave dominance of the decay has actually been used to pin down the quantum numbers of the ω meson [5–8].

If the pions, once produced in the decay, did not interact further, then solely the P-wave phase space would shape the Dalitz plot of the decay $\omega \to \pi^+\pi^-\pi^0$. However, a pion pair in a P-wave shows a very strong final-state interaction. The two-pion P-wave phase shift is dominated by the ρ meson, and is now known very accurately [9–11]; this is essential in particular for theoretical studies of these decays using dispersion theory, which use the phase shifts as input directly [4,12]. In the similar decay $\phi \to \pi^+\pi^-\pi^0$ one can see the ρ meson as a resonance in the corresponding Dalitz plot [13,14]. In the decay $\omega \to \pi^+\pi^-\pi^0$ there is not enough energy for a pion pair to reach the ρ resonance mass; yet already for the available invariant masses the two-pion P-wave phase shift is significantly different from zero. In fact, every theoretical approach that deals with the decay $\omega \to \pi^+\pi^-\pi^0$ includes this non-trivial phase shift and/or the ρ meson in one way or the other; see, *e.g.*, Refs. [15–19,4,20,12] and references therein. In practice this leads to an increase of population towards the boundaries of the Dalitz plot, superimposed with the pure P-wave phase space, which drops towards the boundaries. This increase of population is on the level of about 20% [19,4], and ought to be tested experimentally.

Interestingly this has not been achieved so far. The highest statistics of a dedicated $\omega \to \pi^+\pi^-\pi^0$ Dalitz plot measurement from 1966 had 4208 ± 75 signal events [21]. Due to the limited statistics, fits with a pure P-wave phase space could not be distinguished from a distortion by the final-state interactions, *i.e.* by intermediate $\rho\pi$ states. Surprisingly there were no further dedicated Dalitz plot studies of the $\omega \to \pi^+\pi^-\pi^0$ decay. In the present work we will reveal that the universal final-state interactions of the pion pairs are indeed present in the ω Dalitz decay. In the analysis presented here we have produced an acceptance-corrected Dalitz plot and extracted experimental values for parameters describing the density distribution. This constitutes the first task spelled out in the beginning of this introduction.

The second motivation for a precise measurement of the $\omega \to \pi^+\pi^-\pi^0$ Dalitz plot consists in improving hadronic input for the theoretical assessment of the hadronic light-by-light scattering contribution to the anomalous magnetic moment of the muon. The largest individual contribution is given by the lightest hadronic intermediate state, the so-called π^0 pole term, whose strength is determined by the corresponding singly and doubly virtual transition form factors. One of the few possibilities to gain experimental access to the *doubly* virtual π^0 transition form factor with high precision consists in studying vector meson conversion decays, in

[8] Genuine F-wave corrections have been modelled theoretically, and found to be tiny [4].

particular $\omega \to \pi^0 \ell^+ \ell^-$—which is intimately linked, through dispersion relations, to the $\omega \to \pi^+\pi^-\pi^0$ decay amplitude [22,23,12]. However, these theoretical descriptions of the ω transition form factor (see also Ref. [24]) fail to describe the very precise data on $\omega \to \pi^0 \mu^+ \mu^-$ taken by the NA60 collaboration [25,26], which may violate very fundamental theoretical bounds [27,28]. In all these studies, the $\omega \to \pi^+\pi^-\pi^0$ decay amplitude is a potential loose end, as it is so far only theoretically modelled, not experimentally tested. In combination with the precisely measured $\phi \to \pi^+\pi^-\pi^0$ Dalitz plot information, it could be used to further constrain the amplitude analysis of $e^+e^- \to \pi^+\pi^-\pi^0$, and hence the π^0 transition form factor in a wider range [29].

Recently, an easy-to-use polynomial parametrisation of the $\omega \to \pi^+\pi^-\pi^0$ Dalitz plot distribution has been suggested [4], as a generalisation of the commonly used one for the decay $\eta \to 3\pi^0$ (which has a similar crossing symmetry). In the present work we utilise the same parametrisation and compare to recent theoretical approaches [4,20,12] that have provided predictions for the corresponding Dalitz plot parameters.

One way to describe a three-particle Dalitz decay distribution is to use invariant masses of particle pairs [3]. This would be particularly useful for reading off resonance masses if the decay was mediated by one or several resonances. However, there are no intermediate resonances in the kinematically accessible energy range of the decay $\omega \to \pi^+\pi^-\pi^0$ that would be compatible with the symmetries of the strong interaction. For our case of interest, we first split off the P-wave phase space (see, *e.g.*, Refs. [19,4]) and parametrise the rest by a polynomial distribution following [4]. Denoting the polarisation vector of the ω meson by $\epsilon(P_\omega, \lambda_\omega)$ and the momenta of the outgoing pions by P_+, P_-, and P_0, we start with the most general matrix element compatible with the symmetries,

$$\mathcal{M} = i\varepsilon_{\mu\nu\alpha\beta}\,\epsilon^\mu\, P_+^\nu\, P_-^\alpha\, P_0^\beta\, \mathcal{F}\,. \tag{1}$$

The dynamics of the final-state interactions is encoded in the scalar function $\mathcal{F}$ [19,4]. After summation over the helicity λ_ω of the ω meson one obtains a Dalitz plot distribution proportional to

$$\sum_{\lambda_\omega} |\mathcal{M}|^2 \propto \mathcal{P}\,|\mathcal{F}|^2 \tag{2}$$

with the pure P-wave phase-space distribution

$$\begin{aligned}\mathcal{P} = {} & m_+^2 m_-^2 m_0^2 + 2(P_+P_-)(P_-P_0)(P_0P_+) \\ & - m_+^2 (P_-P_0)^2 - m_-^2 (P_+P_0)^2 - m_0^2 (P_+P_-)^2\,.\end{aligned} \tag{3}$$

Note that for the $\mathcal{P}$ term we can account for "kinematic" isospin violations due to the difference between the masses of the uncharged and charged pions, m_0 and $m_\pm$, respectively. For the remaining distribution $\mathcal{F}$, which covers the dynamics of the final-state interaction, we ignore isospin breaking effects.

The quantity $\mathcal{F}$ and therefore also $|\mathcal{F}|^2$ would be a constant if there were no final-state interactions between the produced pions. In reality $|\mathcal{F}|^2$ is not a constant, but relatively flat. Instead of parameterising $|\mathcal{F}|^2$ by invariant masses of pion pairs we follow Ref. [4] and utilise normalised variables X and Y, which have their origin at the centre of the Dalitz plot. They are defined by

$$X = \sqrt{3}\,\frac{T_+ - T_-}{Q_\omega}, \qquad Y = \frac{3T_0}{Q_\omega} - 1, \tag{4}$$

with

$$Q_\omega = T_+ + T_- + T_0. \tag{5}$$

Here T_i are the kinetic energies of the pions in the ω rest frame (centre-of-mass frame of the three-pion system). Finally one introduces polar coordinates by

Table 1
The Dalitz plot parameters from fits to the theoretical predictions of Refs. [4,20,12], where at most two parameters were used in the fit.

	$\alpha \times 10^3$	$\beta \times 10^3$
Uppsala [20]	202	–
Bonn [4]	84 . . . 102	–
JPAC [12]	94	–
Uppsala	190	54
Bonn	74 . . . 90	24 . . . 30
JPAC	84	28

$$X = \sqrt{Z}\cos\phi, \quad Y = \sqrt{Z}\sin\phi\,. \tag{6}$$

The expansion for $|\mathcal{F}|^2$, valid in the isospin limit, reads

$$|\mathcal{F}|^2(Z,\phi) = \mathcal{N}\cdot\mathcal{G}(Z,\phi)\,, \tag{7}$$

where $\mathcal{N}$ is a normalisation constant and $\mathcal{G}$ contains the expansion in Z and ϕ [4]:

$$\mathcal{G}(Z,\phi) = 1 + 2\alpha Z + 2\beta Z^{3/2}\sin 3\phi + 2\gamma Z^2 + \mathcal{O}\big(Z^{5/2}\big)\,. \tag{8}$$

The Dalitz plot distribution can then be fitted using this formula to extract the "Dalitz plot parameters" α, β, γ, ... The fit results to the theory predictions of Refs. [4,20,12], if Eq. (8) is truncated at order Z (one parameter fit) or at order $Z^{3/2}$ (two parameter fit), are shown in Table 1. The reproduction of the theoretical Dalitz plot distributions is improved significantly in all cases when including the term $\propto \beta$.

It is worth to point out the qualitative similarities and differences of the theoretical approaches that provide predictions for the Dalitz plot parameters. All three approaches agree on a positive and sizable value for α. This reflects the fact that the pion–pion P-wave phase shift is dominated by the appearance of the ρ-meson resonance; an experimental result pointing to a negative value of α would be spectacular in the sense that it would be at odds with the universality of the final-state interactions.

Refs. [4,12] are based on dispersion theory: both employ the pion–pion P-wave scattering phase shift as input and describe rescattering of all three final-state pions consistently to all orders. The dispersive formalism can be chosen with only one single free parameter (a "subtraction constant"), based on reasonable assumptions on the high-energy behaviour of the amplitude; this parameter can be taken to be the overall normalisation and fixed experimentally from the $\omega \to \pi^+\pi^-\pi^0$ partial width. The energy dependence of the decay amplitude is then fully predicted from the pion–pion phase shift alone. The Dalitz plot parameters cited from Ref. [12] in Table 1 are obtained from such a scenario. In Ref. [4], various sources of uncertainty related to the pion–pion interaction have been considered, leading to an estimate of the theoretical error in the prediction of the Dalitz plot parameters. Furthermore, an analysis of data for the analogous $\phi \to \pi^+\pi^-\pi^0$ Dalitz plot [13] demonstrated that a once-subtracted dispersive representation describes such very-high-accuracy data well, but not perfectly, leading to the need to introduce a second subtraction [4]. With such a second free parameter also used in the $\omega \to \pi^+\pi^-\pi^0$ decay amplitude, the energy dependence in principle cannot be entirely predicted any more. However, estimating the size of such a second constant from the $\phi \to \pi^+\pi^-\pi^0$ data analysis, it was found that the uncertainty range for the theoretical prediction of the Dalitz plot parameters is only moderately increased [4]. The ranges quoted in Table 1 reflect this full, combined uncertainty estimate.

Ref. [20] is based on an effective Lagrangian for the lightest pseudoscalar and vector mesons. The strength of the initial ω-ρ-π interaction is fitted to the decay width of $\omega \to \pi^+\pi^-\pi^0$ and cross-checked with the decay width of $\omega \to \pi^0\gamma$. The Lagrangian

provides the kernel for a Bethe–Salpeter equation that generates the two-pion rescattering. In contrast to the dispersive approaches, crossed-channel rescattering of the three-pion system is not included.

While all theory approaches agree on the sign of α, the value predicted by the Lagrangian approach [20] is very different from the values obtained by dispersion theory [4,12]. The same holds true for the β parameter: the larger values from Ref. [20] reflect a rather strong energy dependence of the matrix element. The same qualitative difference can be observed for the electromagnetic transition form factor of $\omega \to \pi^0 \ell^+ \ell^-$ [24,23]: also here the Lagrangian approach provides a much stronger energy dependence. A technical reason for this might be found in the fact that essentially field strengths instead of vector potentials are used for the construction of interaction terms in the Lagrangian approach [19, 24,20]. If the results of this low-energy Lagrangian were boldly extrapolated to high energies—beyond its limit of applicability—, then one would find that the reaction amplitudes would not converge. In contrast, modest high-energy constraints are automatically encoded in the dispersive approaches. Apparently this leads to smaller energy variations of the reaction amplitudes even in the low-energy regime that is of relevance for the ω decays. — At present it is not possible to obtain a serious theoretical uncertainty estimate for the Lagrangian approach [20]. Additional interaction terms have been neglected therein, which were considered to be small, but it is not clear yet how small they are.

2. The experiment

The experimental data was collected using the WASA setup, where the ω was produced in the $pd \to {}^3\mathrm{He}\,\omega$ reaction and in the $pp \to pp\omega$ reaction. The WASA detector [30,31] is an internal target experiment at the Cooler Synchrotron (COSY) storage ring, Forschungszentrum Jülich, Germany. The COSY proton beam interacts with an internal target consisting of small pellets of frozen hydrogen or deuterium (diameter $\sim 35\,\mu\mathrm{m}$).

The WASA detector consists of a Central Detector (CD) and a Forward Detector (FD), covering scattering angles of 20°–169° and 3°–18°, respectively. The CD is used to measure decay products of the mesons. A cylindrical straw chamber (MDC) is placed in a magnetic field of 1 T, provided by a superconducting solenoid. The electromagnetic calorimeter (SEC) consists of 1012 CsI(Na) crystals which are read out by photomultipliers. A plastic scintillator barrel (PSB) is placed between the MDC and the SEC, allowing particle identification and accurate timing for charged particles. The FD consists of thirteen layers of plastic scintillators for energy and time determination and a straw tube tracker providing a precise track direction.

When the ω mesons were produced using the $pd \to {}^3\mathrm{He}\,\omega$ reaction, two different proton kinetic energies were used: $T_A = 1.450\,\mathrm{GeV}$ and $T_B = 1.500\,\mathrm{GeV}$. The cross section of the reaction is 84(10) nb at the lower energy [32] and was studied previously by the CELSIUS/WASA collaboration. Triggers select events with at least one track in the FD with a high energy deposit in the thin plastic scintillator layers. This condition allows for an efficient selection of ^{3}He ions and provides an unbiased data sample of ω meson decays. The proton beam energy was chosen so that the ^{3}He produced in the $pd \to {}^3\mathrm{He}\,\omega$ reaction stops in the second thick scintillator layer of the FD. The correlation plot $\Delta E - \Delta E$ from a thin layer and the first thick layer of the FD is shown in Fig. 1 (top). The band corresponding to the ^{3}He ion is well separated from the bands for other particles and allows a clear identification of ^{3}He. The ^{3}He from the reaction of interest has kinetic energies up to 700 MeV and scattering angles ranging from 0° to 10°.

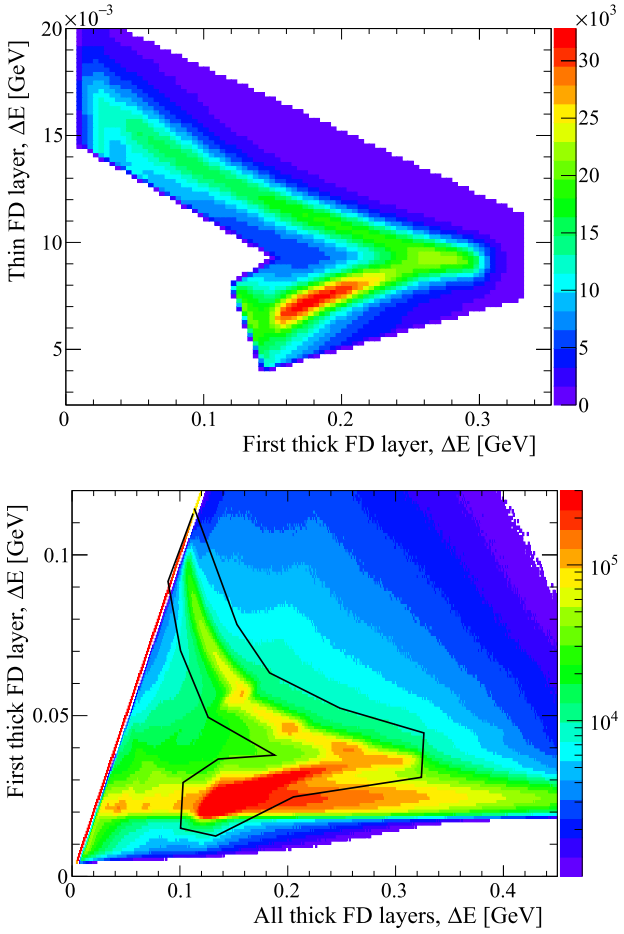

Fig. 1. Particle identification in the Forward Detector is performed using the correlation of energy deposits in the plastic detector layers. (top) For ^{3}He identification: the correlation between the energy deposits in a thin (0.5 cm) layer and the first subsequent thick layer (11 cm). Only the region selected in the analysis is shown in the figure, with the band from ^{3}He particles clearly visible inside it. (bottom) For proton identification: the correlation between the energy deposit in the first thick layer and the summed energy deposits in all thick layers (11 or 15 cm). The correlation band corresponding to energy deposits made by protons is surrounded by the black line. Also visible is a lower, near-horizontal, band which is populated by fast protons punching through the first thick layer, depositing energy of 20 MeV, and undergoing nuclear interaction in one of the subsequent thick layers, there depositing an indefinite amount of energy.

The $pp \to pp\omega$ experiment was performed at $T_C = 2.063\,\mathrm{GeV}$ beam kinetic energy, corresponding to 60 MeV centre-of-mass excess energy and cross section 5.7 µb [33]. In the pp collision experiment, the selected events were required, at trigger level, to contain at least two tracks reaching the second thick layer of the plastic scintillators in the FD, at least two hits in the PSB, and at least one cluster in the SEC. In the offline analysis, pairs of tracks corresponding to the $\Delta E - \Delta E$ proton bands, shown in Fig. 1 (bottom), in different thick layers of the FD are selected as proton pair candidates.

For the particles measured in the CD, a common analysis procedure is used for all three data sets. Events are selected if they contain at least one pair of opposite charge particle tracks in the MDC with scattering angles greater than 30° and at least two neutral clusters with energy deposit above 20 MeV in the SEC. Relative time between the tracks is checked to minimise pile ups. The charged particle tracks are assigned the charged pion mass. Combinations of the all the measured charged and neutral particle tracks in the selected events are tested using a constrained kinematic fit assuming the conservation of energy and momentum

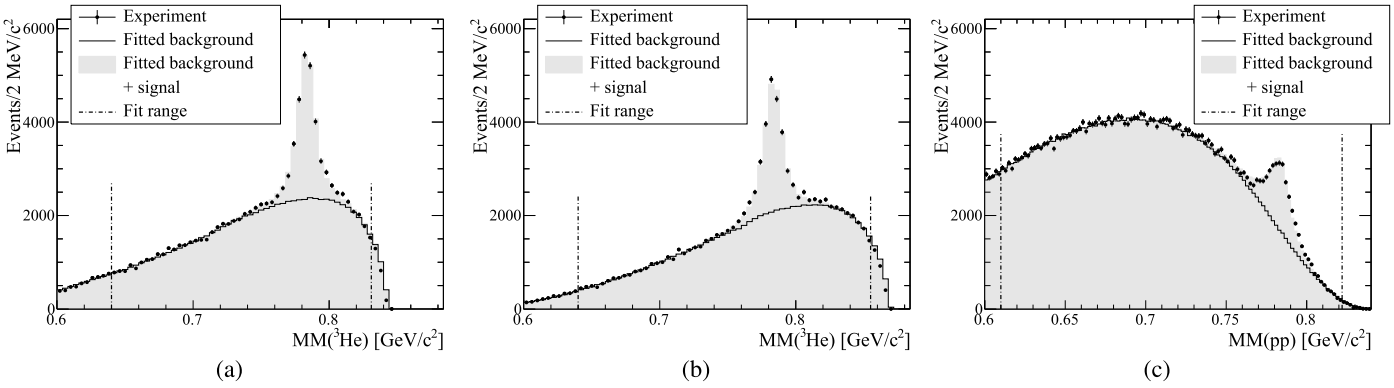

Fig. 2. Missing mass distributions after the full analysis procedure as well as the result of the fit Eq. (9). (a): $T_A = 1.450\,\text{GeV}$. (b): $T_B = 1.500\,\text{GeV}$. (c): $T_C = 2.063\,\text{GeV}$.

with the $pd \to {}^3\text{He}\,\pi^+\pi^-\gamma\gamma$ or $pp \to pp\pi^+\pi^-\gamma\gamma$ hypothesis, respectively. The combinations with p-values less than 0.05 are rejected. For the case when more than one track combination in an event fulfils this criteria, the combination giving larger p-value is selected. Finally, further background suppression is achieved by applying a kinematic fit with the contending hypothesis $pd \to {}^3\text{He}\,\pi^+\pi^-$ or $pp \to pp\pi^+\pi^-$, respectively. If the resulting p-value is larger than for the first fit, the event is rejected.

The missing mass distributions, MM(^{3}He) and MM(pp), for the three data sets are shown in Fig. 2. The missing masses, calculated from the variables corrected by the kinematic fit, are equivalent to the invariant mass of the $\pi^+\pi^-\gamma\gamma$ system. The observed ω peak position is shifted from the nominal value of the ω mass by $+0.7\,\text{MeV}$ for MM(^{3}He) in the two pd data sets and by $+1.1\,\text{MeV}$ for MM(pp). The observed shifts correspond to deviations from the nominal beam energy by 0.55 MeV and 0.75 MeV, respectively, which is well within the uncertainty of the absolute energy scale of COSY. To reproduce the experimental ω peak position, the missing mass distributions from simulated data were shifted accordingly. To also reach agreement between experiment and simulation for the width of the ω peak, the resolution from simulated detector responses were adjusted.

Both the background shape and the ω peak content are fitted simultaneously to the experimental distribution using the following fit function:

$$H(\mu) = N_S H_\omega(\mu) + \left\{a_0 + a_1\mu + a_2\mu^2 + a_3\mu^3\right\} \times H_{3\pi}(\mu), \quad (9)$$

where $\mu = \text{MM}(^3\text{He})$ or MM(pp). $H_\omega(\mu)$ and $H_{3\pi}(\mu)$ represent reconstructed distributions of simulated signal and background and correspond to events that have passed through the same analysis steps as the experimental data. $H_\omega(\mu)$ is normalised such that the fit gives directly the number of signal events, N_S, and the related error. The other parameters fitted are a_0, a_1, a_2, and a_3 (in case of pd data a_3 is set to 0). The range in μ used for the fit is $[0.640, 0.832]\,\text{GeV/c}^2$ for set A, $[0.640, 0.856]\,\text{GeV/c}^2$ for set B, and $[0.608, 0.824]\,\text{GeV/c}^2$ for set C. The limits of these ranges are shown by the dashed lines in Fig. 2, where the result of these fits to the full data samples are given. The resulting number of events is: 14600(200) for set A, 13500(200) for set B, and 16000(300) for set C.

3. Dalitz plot

The Dalitz plot density is represented using a two-dimensional histogram in the Z and ϕ variables, defined in Eq. (6). The size of the selected bins is determined by the experimental resolution of Z and ϕ and the statistics of the collected data sample. The number of events in each bin should be sufficient for determining

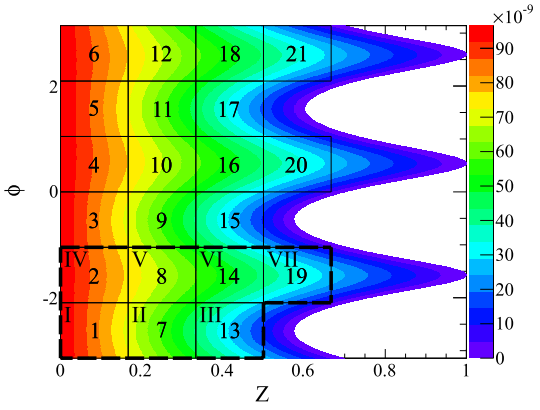

Fig. 3. The Arabic numerals show the bin numbers to be used when presenting the resulting Dalitz plots. The colour plot shows the kinematically allowed region of the $\omega \to \pi^+\pi^-\pi^0$ reaction with ω nominal mass as well as the density distribution from P-wave dynamics. The Roman numerals display the sectors used in consistency checks.

the signal yield and to carry out a χ^2 fit of the Dalitz plot density parametrisation. The ϕ variable range $[-\pi, \pi]$ is divided into six bins to preserve the threefold isospin symmetry and to be sensitive to a possible $\sin 3\phi$ dependence. The Z variable range $[0, 1]$ is also divided into six bins. Only the 21 bins fully contained inside the kinematic limits of the decay are used. Fig. 3 introduces the bin numbering used for the presentation of the results.

A small shift of the Dalitz plot along the Y axis is due to the mass difference between the neutral and charged pions. It is most visible in Fig. 3 when comparing the regions at $\phi = \pi/2$ to the ones at $\phi = -\pi/6$ and $-2\pi/3$. The picture shows also seven sectors I–VII that are used to test the consistency of the fit results.

For each Dalitz plot bin, the experimental missing mass distribution is constructed and the number of entries in the ω peak is extracted by fitting a simulated $\omega \to \pi^+\pi^-\pi^0$ signal along with background contributions using Eq. (9).

Since the P-wave distribution reproduces the general features of the $\omega \to \pi^+\pi^-\pi^0$ Dalitz plot very well and the deviations are expected to be small, the efficiency correction is obtained using signal simulation with the P-wave. The efficiency, ϵ_i, is extracted using the ratio $\epsilon_i = N_i/N_i^G$. N_i^G is the number of events with generated kinematic variables corresponding to bin i in the Dalitz plot. N_i is the content of the bin i when the reconstructed values of the kinematic variables are used for events passing all analysis steps. The extracted efficiencies for the three data sets are shown in Fig. 4. For the pd data sets the overall efficiency is 11%, while for pp it is 20 times lower. This low efficiency for the pp data sample has the following well-understood causes. In most cases,

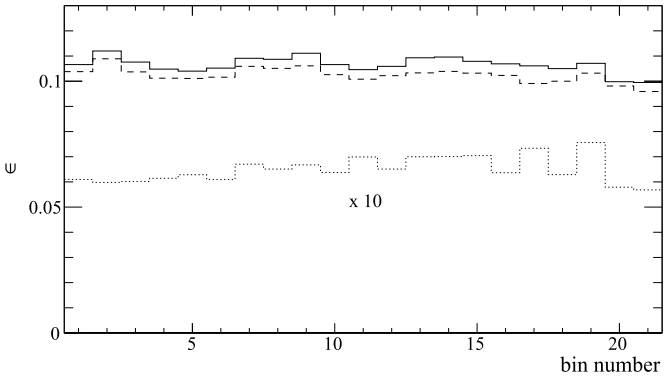

Fig. 4. The resulting efficiencies for each Dalitz plot bin for the three data sets. The relation between the bin numbers used here and the bins of the two-dimensional Dalitz plot is shown in Fig. 3. The solid line corresponds to set A, the dashed line to set B, and the dotted line is the acceptance for the *pp* data set C, which is multiplied by a factor of 10.

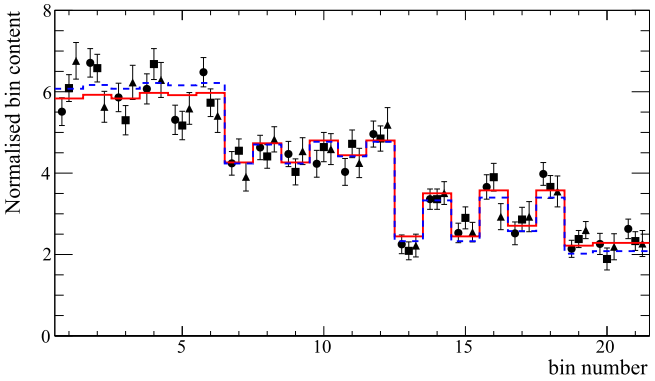

Fig. 5. The experimental Dalitz plot distribution after applying an efficiency correction. The relation between the bin numbers used here and the bins of the two-dimensional Dalitz plot is shown in Fig. 3. Circles correspond to set A, squares to set B, and triangles to set C. The solid red line is the standard fit result (with α parameter), and the dashed line is P-wave only.

the two fast proton tracks deposit only a fraction of their kinetic energy in the detector, leading to a lower precision of the kinetic energy determination and an asymmetric resolution function. The events from the tails will likely be rejected by the kinematic fit procedure. On the other hand for the $pd \to {}^3\mathrm{He}\,\omega$ reaction, there is only one doubly charged ^{3}He stopping in the detector. Another cause for the low efficiency is the larger centre-of-mass velocity in the *pp* reaction, which decreases the average emission angle for decay particles, in particular for the charged pions. The pions will be more often emitted at angles below 30° and will therefore be rejected in the analysis procedure.

The Dalitz plot parameters (α, β, ...) and normalisation factors for the three data sets ($\mathcal{N}_A$, $\mathcal{N}_B$, $\mathcal{N}_C$) are determined by minimising the following $\chi^2 = \chi^2_A + \chi^2_B + \chi^2_C$ function, where

$$\chi^2_A = \sum_i \left(\frac{\tilde{N}_{iA} - \mathcal{N}_A \cdot H_i(\alpha, \beta, \ldots)}{\tilde{\sigma}_{iA}} \right)^2 . \qquad (10)$$

$\tilde{N}_i$ and $\tilde{\sigma}_i$ are the efficiency corrected experimental Dalitz plot bin content and error, respectively. H_i is given by an integral over bin i: $H_i(\alpha, \beta, \ldots) = \int_i \mathcal{P}(Z,\phi)\mathcal{G}(Z,\phi)dZd\phi$. $\mathcal{P}(Z,\phi)$ is the P-wave phase space term given by Eq. (3), calculated using the nominal mass of the ω meson of 782.65 MeV, and $\mathcal{G}(Z,\phi)$ is given by Eq. (8).

The parametrisation procedure of the Dalitz plot is tested using 10^6 signal events simulated with P-wave phase space only (*i.e.* $\mathcal{G} = 1$) and without detector smearing. The extracted parameters are found to be consistent with zero and therefore the procedure does not introduce any bias at the present statistical accuracy.

The three independent data sets and the Dalitz plot symmetries allow for detailed checks of the experimental efficiency and the background subtraction procedure since the background distributions and efficiencies are different in the corresponding bins.

The method of background subtraction for the missing mass μ distributions is tested by preparing simulated distributions after full detector reconstruction, consisting of a sum of $\pi^+\pi^-\pi^0$ production background events and the ω signal generated using a P-wave phase space distribution. The background is obtained from the $\{a_0 + a_1\mu + a_2\mu^2 + a_3\mu^3\} \times H_{3\pi}(\mu)$ distributions with a_i determined from the fits using Eq. (9) and by setting the average signal-to-background ratio to be the same as in the experimental data. The generated μ distributions with the number of events similar as in the experiment are then subjected to the same background subtraction as the experimental data. The combined fit of

Table 2
Dalitz plot bin content for the three data sets. The relative normalisation between the sets is based on the normalisation factors ($\mathcal{N}_A$, $\mathcal{N}_B$, $\mathcal{N}_C$) obtained from individual fits of the α parameter to the three data sets. The overall normalisation factor is arbitrary.

bin#	set A	set B	set C
1	5.51(34)	6.09(33)	6.76(45)
2	6.71(35)	6.58(34)	5.63(38)
3	5.86(35)	5.30(36)	6.23(42)
4	6.07(37)	6.68(38)	6.29(43)
5	5.31(36)	5.17(35)	5.59(39)
6	6.48(36)	5.73(34)	5.41(41)
7	4.24(29)	4.55(29)	3.91(35)
8	4.63(30)	4.41(29)	4.83(31)
9	4.47(31)	4.03(32)	4.54(33)
10	4.23(33)	4.64(36)	4.59(38)
11	4.03(33)	4.72(34)	4.25(36)
12	4.96(32)	4.85(31)	5.19(42)
13	2.25(23)	2.09(22)	2.22(28)
14	3.36(25)	3.36(25)	3.51(28)
15	2.53(24)	2.90(27)	2.55(24)
16	3.66(30)	3.90(34)	2.93(32)
17	2.52(28)	2.86(30)	2.93(37)
18	3.98(28)	3.66(28)	3.55(38)
19	2.14(21)	2.38(21)	2.60(21)
20	2.26(26)	1.89(27)	2.19(32)
21	2.63(24)	2.33(23)	2.27(32)

the Dalitz plot parametrisation to the samples A and B with only the α parameter gives $\alpha = (10 \pm 35) \cdot 10^{-3}$ and $\chi^2 = 36/39$. For set C $\alpha = (25 \pm 59) \cdot 10^{-3}$ and $\chi^2 = 24/19$. Therefore the background subtraction procedure does not introduce any experimental bias.

One can also study the bias and accuracy of the efficiency determination by considering X- or Y-dependent corrections for the efficiency: $\epsilon_i \to \epsilon_i \cdot (1 + \xi_A X)$ or $\epsilon_i \to \epsilon_i \cdot (1 + \zeta_A Y)$, where $\xi_{A,\ldots}$, $\zeta_{A,\ldots}$ are single parameters for each data set. Fits to separate data sets show that all ζ coefficients are consistent with zero and do not change the value of the χ^2. On the other hand, ξ_B and ξ_C were found to significantly deviate from zero, although with opposite signs. Applying these two corrections to the efficiency before a fit of the Dalitz plot parametrisation yields a significantly reduced χ^2 value. However, the determined values of the Dalitz parameters are not affected, *e.g.* $\alpha = (147 \pm 35) \cdot 10^{-3}$ and $\alpha = (147 \pm 36) \cdot 10^{-3}$ without and with correction, respectively. This comes from the fact that the fitted parametrisation is preserving isospin symmetry. In conclusion, we apply the X-dependent corrections to the efficiency corrections of data sets B and C, as it ensures the anticipated charge symmetry of the Dalitz plot and leads to a decrease

Table 3
The resulting Dalitz plot parameters after a individual fits to the three data sets, where at most two parameters were used in the fit.

Data set	$\alpha \times 10^3$	$\beta \times 10^3$	χ^2/d.o.f.
A	–	–	28.7/20
	142(59)	–	22.2/19
	102(66)	109(87)	20.7/18
B	–	–	35.4/20
	146(59)	–	28.5/19
	154(69)	−21(92)	28.5/18
C	–	–	26.5/20
	154(69)	–	20.8/19
	149(78)	14(102)	20.8/18

Table 4
Dalitz plot parameters from simultaneous fits to the three data sets, where at most two parameters were used in the fit.

$\alpha \times 10^3$	$\beta \times 10^3$	χ^2/d.o.f.
–	–	90.6/60
147(36)	–	71.5/59
133(41)	37(54)	71.0/58

of the χ^2 as well as the correct statistical significance when fitting the Dalitz parameters. The resulting efficiency corrected and normalised Dalitz plot bin contents are provided in Table 2.

The extracted Dalitz plot parameters and goodness of fit for each data set separately are reported in Table 3. There is a significant decrease of the χ^2 value when including the α parameter and the results from the three data sets are consistent. The results of the fits for all data sets combined are given in Table 4. The p-value significantly improves after including the α parameter, while inclusion of an additional parameter does not improve the p-value any further. The efficiency corrected Dalitz plots for the three data sets are shown in Fig. 5, where they are compared to the P-wave distribution as well as the fit with the α parameter. We consider the result with the α parameter our main finding. The difference between the results from the first and second fits in Table 4 indicates the onset of dynamics in the reaction on top of the P-wave phase space distribution. This follows the expected behaviour of an increase towards the edges of phase space due to the attractive $\pi\pi$ final-state interaction (approaching the ρ resonance), yielding a positive value for the α parameter.

Fig. 6 shows a test of data consistency for the same Dalitz plot sectors, marked with Roman numerals in Fig. 3. Arithmetical averages of the normalised residuals with respect to the α parameter fit from bins corresponding to the same sectors are calculated for the separate data sets and for all three data sets combined. The error bars correspond to the calculated root mean square values, which are expected to be 1 for a random data sample with correctly estimated uncertainties.

Here follows a short summary of the checks for systematic effects reported in this section. Two input–output checks were performed, which verified that the parametrisation procedure as well as the method of background subtractions does not introduce any bias at the present statistical accuracy. The efficiency correction was checked and adjusted to ensure charge symmetry in the Dalitz plot. Lastly, the consistency between the three data sets as well as the different sectors of the Dalitz plot was checked. The result from these checks is that the accuracy of the Dalitz plot parameters is dominated by statistic uncertainty.

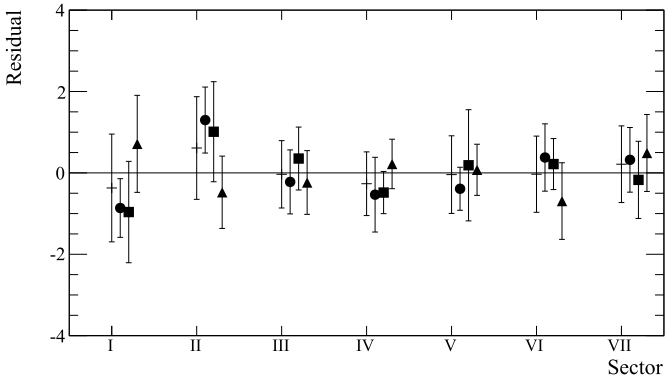

Fig. 6. Arithmetic averages and root mean square of the normalised residuals in separate Dalitz plot sectors for all data sets (crosses) and for the separate data sets (A – circles, B – squares, C – triangles) for the standard fit.

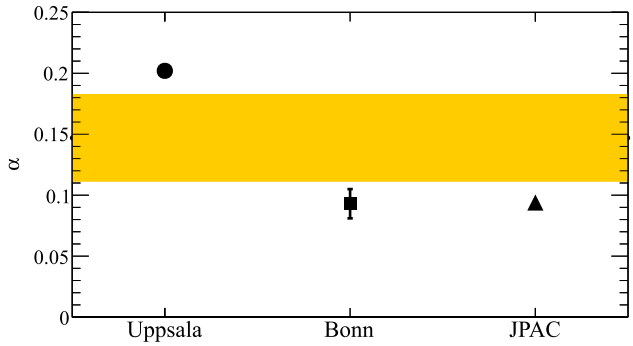

Fig. 7. Comparison of our result for the α parameter (shaded area) with the three theoretical predictions [20,4,12].

4. Summary and discussion

For the first time a deviation from a pure P-wave distribution in $\omega \to \pi^+\pi^-\pi^0$ is observed and quantified by the determination of the parameter $\alpha = (147 \pm 36) \cdot 10^{-3}$, *i.e.* a positive value with 4.1σ significance. Fig. 7 compares the experimental result of the α parameter to the theoretical predictions. The experimental α value is clearly in the vicinity of the predictions made by dispersion theory [4,12] and the effective-Lagrangian approach [20]. However the experimental uncertainty is still too sizeable to allow for definite conclusions concerning the validity of these contrasting predictions. The systematic effects were studied by comparing three data sets using two production reactions, which differ significantly in resolution and acceptance. The chosen Z, ϕ parametrisation together with isospin symmetry allows for more tests of systematic effects, and the precision of the result is dominated by the statistical uncertainty.

Acknowledgements

This work was supported in part by the EU Integrated Infrastructure Initiative HadronPhysics Project under contract number RII3-CT-2004-506078; by the European Commission under the 7th Framework Programme through the Research Infrastructures action of the Capacities Programme, Call: FP7-INFRASTRUCTURES-2008-1, Grant Agreement N. 227431; by the Polish National Science Centre through the grants DEC-2013/11/N/ST2/04152, 2011/01/B/ST2/00431, 2011/03/B/ST2/01847, and the Foundation for Polish Science (MPD), co-financed by the European Union within the European Regional Development Fund. We gratefully acknowledge the support given by the Swedish Research Council,

the Knut and Alice Wallenberg Foundation, and the Forschungszentrum Jülich FFE Funding Program. This work is based on the PhD theses of Lena Heijkenskjöld and Siddhesh Sawant.

References

[1] G. Colangelo, M. Hoferichter, B. Kubis, M. Procura, P. Stoffer, Phys. Lett. B 738 (2014) 6–12, arXiv:1408.2517.
[2] B.C. Maglić, L.W. Alvarez, A.H. Rosenfeld, M.L. Stevenson, Phys. Rev. Lett. 7 (1961) 178–182;
B.C. Maglić, L.W. Alvarez, A.H. Rosenfeld, M.L. Stevenson, Adv. Exp. Phys. 5 (1976) 106.
[3] K.A. Olive, et al., Particle Data Group, Chin. Phys. C 38 (2014) 090001.
[4] F. Niecknig, B. Kubis, S.P. Schneider, Eur. Phys. J. C 72 (2012) 2014, arXiv:1203.2501.
[5] M.L. Stevenson, L.W. Alvarez, B.C. Maglić, A.H. Rosenfeld, Phys. Rev. 125 (1962) 687–690.
[6] C. Alff, et al., Phys. Rev. Lett. 9 (1962) 325–327.
[7] N.-h. Xuong, G.R. Lynch, Phys. Rev. 128 (1962) 1849–1867.
[8] J.S. Danburg, M.A. Abolins, O.I. Dahl, D.W. Davies, P.L. Hoch, J. Kirz, D.H. Miller, R.K. Rader, Phys. Rev. D 2 (1970) 2564–2588.
[9] B. Ananthanarayan, G. Colangelo, J. Gasser, H. Leutwyler, Phys. Rep. 353 (2001) 207–279, arXiv:hep-ph/0005297.
[10] G. Colangelo, J. Gasser, H. Leutwyler, Nucl. Phys. B 603 (2001) 125–179, arXiv:hep-ph/0103088.
[11] R. García-Martín, R. Kamiński, J.R. Peláez, J. Ruiz de Elvira, F.J. Ynduráin, Phys. Rev. D 83 (2011) 074004, arXiv:1102.2183.
[12] I.V. Danilkin, C. Fernández-Ramírez, P. Guo, V. Mathieu, D. Schott, M. Shi, A.P. Szczepaniak, Phys. Rev. D 91 (2015) 094029, arXiv:1409.7708.
[13] A. Aloisio, et al., KLOE, Phys. Lett. B 561 (2003) 55–60, arXiv:hep-ex/0303016;
A. Aloisio, et al., KLOE, Phys. Lett. B 609 (2005) 449 (Erratum).
[14] R.R. Akhmetshin, et al., Phys. Lett. B 642 (2006) 203–209.
[15] M. Gell-Mann, D. Sharp, W.G. Wagner, Phys. Rev. Lett. 8 (1962) 261.
[16] F. Klingl, N. Kaiser, W. Weise, Z. Phys. A 356 (1996) 193–206, arXiv:hep-ph/9607431.
[17] M. Harada, K. Yamawaki, Phys. Rep. 381 (2003) 1–233, arXiv:hep-ph/0302103.
[18] P.D. Ruiz-Femenía, A. Pich, J. Portolés, J. High Energy Phys. 07 (2003) 003, arXiv:hep-ph/0306157.
[19] S. Leupold, M.F.M. Lutz, Eur. Phys. J. A 39 (2009) 205–212, arXiv:0807.4686.
[20] C. Terschlüsen, B. Strandberg, S. Leupold, F. Eichstädt, Eur. Phys. J. A 49 (2013) 116, arXiv:1305.1181.
[21] S.M. Flatté, D.O. Huwe, J.J. Murray, J. Button-Shafer, F.T. Solmitz, M.L. Stevenson, C. Wohl, Phys. Rev. 145 (1966) 1050–1061.
[22] G. Köpp, Phys. Rev. D 10 (1974) 932–940.
[23] S.P. Schneider, B. Kubis, F. Niecknig, Phys. Rev. D 86 (2012) 054013, arXiv:1206.3098.
[24] C. Terschlüsen, S. Leupold, Phys. Lett. B 691 (2010) 191–201, arXiv:1003.1030.
[25] R. Arnaldi, et al., NA60, Phys. Lett. B 677 (2009) 260–266, arXiv:0902.2547.
[26] R. Arnaldi, et al., NA60, Phys. Lett. B 757 (2016) 437–444.
[27] B. Ananthanarayan, I. Caprini, B. Kubis, Eur. Phys. J. C 74 (2014) 3209, arXiv:1410.6276.
[28] I. Caprini, Phys. Rev. D 92 (2015) 014014, arXiv:1505.05282.
[29] M. Hoferichter, B. Kubis, S. Leupold, F. Niecknig, S.P. Schneider, Eur. Phys. J. C 74 (2014) 3180, arXiv:1410.4691.
[30] H.H. Adam, et al., WASA-at-COSY, arXiv:nucl-ex/0411038, 2004.
[31] C. Bargholtz, et al., CELSIUS/WASA, Nucl. Instrum. Methods, Sect. A 594 (2008) 339–350, arXiv:0803.2657.
[32] K. Schönning, et al., CELSIUS/WASA, Phys. Rev. C 79 (2009) 044002, arXiv:0902.3905.
[33] S. Barsov, et al., Eur. Phys. J. A 31 (2007) 95–104, arXiv:nucl-ex/0609010.